

Degradation-Aware Frequency Regulation of a Heterogeneous Battery Fleet via Reinforcement Learning

Tanay Raghunandan
 Srinivasa
 Plaksha University
 Mohali, India
 tanay.srinivasa@plaksha.edu.in

Vivek Deulkar
 Plaksha University
 Mohali, India
 vivek.deulkar@plaksha.edu.in

Jia Bhargava
 Plaksha University
 Mohali, India
 jia.bhargava@plaksha.edu.in

Mohammad Hajiesmaili
 University of Massachusetts
 Amherst
 Amherst, United States of
 America
 hajiesmaili@cs.umass.edu

Prashant Shenoy
 University of Massachusetts
 Amherst
 Amherst, United States of
 America
 shenoy@cs.umass.edu

ABSTRACT

Battery energy storage systems are increasingly deployed as fast-responding resources for grid balancing services such as frequency regulation and for mitigating renewable generation uncertainty. However, repeated charging and discharging induces cycling degradation and reduces battery lifetime. This paper studies the real-time scheduling of a heterogeneous battery fleet that collectively tracks a stochastic balancing signal subject to per-battery ramp-rate and capacity constraints, while minimizing long-term cycling degradation.

Cycling degradation is fundamentally path-dependent: it is determined by charge–discharge cycles formed by the state-of-charge (SoC) trajectory and is commonly quantified via rainflow cycle counting. This non-Markovian structure makes it difficult to express degradation as an additive per-time-step cost, complicating classical dynamic programming approaches. We address this challenge by formulating the fleet scheduling problem as a Markov decision process (MDP) with constrained action space and designing a dense proxy reward that provides informative feedback at each time step while remaining aligned with long-term cycle-depth reduction.

To scale learning to large state–action spaces induced by fine-grained SoC discretization and asymmetric per-battery constraints, we develop a function-approximation reinforcement learning method using an Extreme Learning Machine (ELM) as a random nonlinear feature map combined with linear temporal-difference learning. We evaluate the proposed

approach on a toy Markovian signal model and on a Markovian model trained from real-world regulation signal traces obtained from the University of Delaware, and demonstrate consistent reductions in cycle-depth occurrence and degradation metrics compared to baseline scheduling policies.

CCS CONCEPTS

- Applied computing → Economics; Decision analysis;

KEYWORDS

Battery degradation, frequency regulation, reinforcement learning, Markov decision processes, Extreme Learning Machines, stochastic control

ACM Reference Format:

Tanay Raghunandan Srinivasa, Vivek Deulkar, Jia Bhargava, Mohammad Hajiesmaili, and Prashant Shenoy. . Degradation-Aware Frequency Regulation of a Heterogeneous Battery Fleet via Reinforcement Learning. In . ACM, New York, NY, USA, 12 pages.

1 INTRODUCTION

Power system operators increasingly rely on fast-responding energy storage resources to provide frequency regulation and other ancillary services. Battery energy storage systems (BESSs), in particular, are well suited for frequency regulation due to their rapid ramping capabilities, high round-trip efficiency, and modular deployability [11]. In practice, frequency regulation is often provided not by a single large battery, but by an aggregated fleet of heterogeneous battery units that collectively track a regulation signal provided by the system operator [7, 10].

Despite their operational advantages, batteries suffer from cycling-induced degradation [12, 22], which significantly affects their lifetime and long-term economic viability. A central challenge in operating battery fleets for frequency regulation is therefore to balance regulation performance with degradation minimization. This challenge is compounded by two fundamental characteristics of the problem. First, battery fleets are heterogeneous: individual units may differ in

Permission to make digital or hard copies of all or part of this work for personal or classroom use is granted without fee provided that copies are not made or distributed for profit or commercial advantage and that copies bear this notice and the full citation on the first page. Copyrights for components of this work owned by others than ACM must be honored. Abstracting with credit is permitted. To copy otherwise, or republish, to post on servers or to redistribute to lists, requires prior specific permission and/or a fee. Request permissions from permissions@acm.org.

© Association for Computing Machinery.

energy capacity, ramping limits, and current state of charge (SoC). Second, degradation is path-dependentit depends not only on instantaneous charge or discharge actions, but on the entire sequence of actions that shape the SoC trajectory over time.

In this work, we study the problem of operating a fleet of N heterogeneous battery units to provide frequency regulation while minimizing long-term cycling degradation. The regulation signal is modeled as a discrete-time stochastic process evolving over a finite state space, capturing the uncertainty and temporal correlation inherent in regulation demand. At each time slot, the aggregator must decide how to distribute the regulation request across the battery units, subject to per-battery energy capacity and ramping constraints, as well as collective feasibility constraints. These decisions determine the evolution of each battery's SoC and, consequently, the cycle formation patterns that drive degradation.

A key difficulty in this setting is that battery degradation cannot be expressed as a simple additive cost per time step. Instead, degradation is commonly modeled using cycle-counting methods such as the rainflow counting algorithm [3] which identify charge-discharge cycles from SoC trajectories and assign damage based on cycle depth. Even though such models are accurate (see [12, 22]), they are inherently non-Markovian and do not naturally admit an incremental per-step cost representation. This poses a major obstacle to applying standard optimization and control techniques, including dynamic programming.

To address this challenge, we adopt a reinforcement learning (RL) framework. RL is particularly well suited to this problem for multiple reasons. The regulation signal dynamics are modeled as a Markov process with unknown transition probabilities, making model-free learning attractive. The control decisions influence degradation through long-term SoC trajectories rather than instantaneous effects, requiring a method capable of reasoning over extended horizons. Also, the action space is state-dependent and constrained by physical battery limits, further complicating classical approaches.

However, applying RL in this context introduces its own challenges. One of the major challenges is to design a reward function that incentivizes the agent to shape SoC trajectories in a degradation-aware manner, despite the delayed and path-dependent nature of true cycling damage. Directly using cycle-based degradation as a reward leads to sparse and delayed reward, which is poorly suited for learning. Consequently, an appropriate reward-shaping strategy is required that provides informative intermediate feedback while remaining aligned with long-term degradation minimization.

In this paper, we propose a degradation-aware RL framework for frequency regulation using heterogeneous battery fleets. We formulate the problem as a Markov decision process (MDP) and introduce a dense proxy reward design derived from real-time properties of SoC trajectories that encourages shallow cycling and avoids deep cycle discharge. The learned policy is evaluated using the full rainflow cycle counting to quantify the actual degradation, ensuring

that performance is assessed using a physically meaningful metric.

To scale learning to large state and action spaces, we employ a function approximation to estimate Q -functions. Specifically, we use an Extreme Learning Machine (ELM) as a random nonlinear feature map over state-action pairs, and learn a linear value function using semi-gradient temporal-difference updates. This approach enables efficient learning while retaining nonlinear representational capabilities.

Our Contributions

The main contributions of this paper are as follows:

- We formulate the operation of heterogeneous battery fleets for frequency regulation as a discrete-time MDP with stochastic regulation demand, explicit ramping and capacity constraints, and long-term degradation objectives.
- We develop a dense reward-shaping mechanism that guides the RL agent toward SoC trajectories with reduced cycling depth, while remaining aligned with cycle-based degradation models that detect cycles and associated degradation only over long time horizons.
- We propose an RL solution based on random feature extraction using Extreme Learning Machines combined with linear temporal-difference learning for value-function approximation.
- We evaluate the proposed approach using realistic regulation signals and quantify performance using rainflow-based degradation metrics, demonstrating significant reductions in cycling damage compared to baseline dispatch strategies.

Related Work

Data-driven methods, and reinforcement learning (RL) in particular, have made substantial progress in solving sequential decision-making problems. The introduction of neural networks as function approximators in RL, popularized by the seminal work in [13], demonstrated that model-free learning can scale to large and complex state spaces. Since then, RL has been widely applied in energy systems, including demand response [18], energy management, and storage control such as electric vehicle charging scheduling [19] and energy arbitrage using battery storage [20, 21]. While these studies demonstrate the flexibility of RL in handling uncertainty and complex system dynamics, battery degradation is either ignored altogether or typically modeled in a simplified manner and do not capture the cycle-dependent aging behavior that is critical for applications involving frequent charge-discharge operation, such as frequency regulation.

The works in [12, 22] rigorously study battery degradation using both physics-based and data-driven techniques, offering models that account for cycle-based degradation. [24] uses machine learning to identify degradation patterns.

There are recent work that has tried to bridge the gap between RL-based control and cycle-based degradation [2, 5,

[9, 23]. [9] formulate frequency regulation with battery storage as an MDP in which regulation tracking performance and cycling degradation are combined into an additive cost function. Their approach augments the state with multiple recent switching points of the state-of-charge (SoC) trajectory to infer cycle formation. In contrast, our formulation enforces frequency regulation requirements as hard feasibility constraints and relies only on the most recent switching point to construct a degradation-aware reward, enabling simpler state representation and online implementation. The work in [2] incorporate battery degradation into RL by introducing a linearized approximation of cycle-based degradation as an instantaneous per-step cost. However, this requires the entire episode data trace for linearization and must be updated episodically. This sensitivity to the chosen trajectory can lead to modeling mismatch and may limit the ability of the learning algorithm to explore and converge to optimal policies over the full policy space.

Overall, while prior work has demonstrated the potential of reinforcement learning for energy storage operation and has explored various approaches to modeling battery degradation, effectively incorporating accurate, cycle-based degradation into scalable, online RL frameworks for frequency regulation remains an open problem. The present work addresses this gap by designing a degradation-aware reward that is compatible with real-time learning and by developing a stable function-approximation-based RL approach for a heterogeneous battery fleet.

2 MODEL AND PROBLEM FORMULATION

We consider the operation of an aggregator controlling a fleet of N heterogeneous battery energy storage units to provide frequency regulation over a discrete-time horizon. Time is slotted as $t = 0, 1, 2, \dots$ with each slot corresponding to a fixed duration Δ .

2.1 Frequency Regulation Signal Model

Let $r(t) \in \mathbb{Z}$ denote the frequency regulation request at time slot t , measured in units of energy over the slot duration. Positive values of $r(t)$ correspond to a request for net charging (absorbing energy from the grid), while negative values correspond to a request for net discharging (injecting energy into the grid). Due to fine-grained energy measurement and discretization, all quantities in the system including battery energy levels, ramping limits, and regulation requests are assumed to be integer-valued.

The regulation signal is modeled as an exogenous stochastic process with unknown dynamics. To obtain a finite-state MDP amenable to reinforcement learning, we approximate the signal evolution using a discrete-time Markov chain (DTMC) over a finite state space \mathcal{S}_r , with unknown transition probabilities. This model captures both the stochastic nature of regulation demand and its temporal correlation, while allowing for model-free learning.

2.2 Battery Model and Local Constraints

Each battery unit $i \in \{1, \dots, N\}$ is characterized by the following parameters: energy capacity $B_i \in \mathbb{Z}_+$, maximum charging rate $c_i \in \mathbb{Z}_+$, maximum discharging rate $d_i \in \mathbb{Z}_+$. Recall that we measure energy with fine granularity and, consequently, all of these quantities are represented as integer values. This discretization does not affect modeling fidelity.

Let $b_i(t) \in \{0, 1, \dots, B_i\}$ denote the state of charge (SoC) of battery i at the beginning of time slot t . During slot t , the aggregator agent selects an action $a_i(t) \in \mathbb{Z}$, where $a_i(t) > 0$ represents charging and $a_i(t) < 0$ represents discharging. The per-battery action is constrained by both ramping limits and energy availability:

$$-\min\{d_i, b_i(t)\} \leq a_i(t) \leq \min\{c_i, B_i - b_i(t)\}, \quad (1)$$

where $c_i, d_i > 0$ represent maximum possible charging and discharging in one time step. The SoC then evolves deterministically according to

$$b_i(t+1) = b_i(t) + a_i(t), \quad (2)$$

ensuring that the battery energy level never exceeds its capacity or falls below zero.

2.3 Collective Feasibility and Regulation Tracking

At each time slot, the battery fleet must collectively track the regulation request as closely as possible, subject to physical feasibility. We define the aggregate feasible charging and discharging limits at time t as

$$A_{\max}(t) = \sum_{i=1}^N \min\{c_i, B_i - b_i(t)\}, \quad A_{\min}(t) = -\sum_{i=1}^N \min\{d_i, b_i(t)\}. \quad (3)$$

The maximum regulation that can be served by the fleet is therefore bounded within $[A_{\min}(t), A_{\max}(t)]$. We define the served regulation

$$\tilde{r}(t) = \text{clip}(r(t), A_{\min}(t), A_{\max}(t)), \quad (4)$$

where

$$\text{clip}(x, \ell, u) = \min\{\max\{x, \ell\}, u\}. \quad (5)$$

The action vector $a(t) = (a_1(t), \dots, a_N(t))$ must satisfy the collective constraint

$$\sum_{i=1}^N a_i(t) = \tilde{r}(t), \quad (6)$$

in addition to the per-battery constraints described in Section 2.2. The set of admissible actions at state $s(t)$ is therefore state-dependent and denoted by $\mathcal{A}_{s(t)}$.

This formulation ensures that the fleet provides the maximum feasible regulation at every time step, while allowing the learning agent to decide how the regulation burden is distributed across individual batteries.

We consider a scenario involving multiple battery storage units¹ operated in the presence of a stochastic frequency regulation signal $r(t)$. When the regulation signal is positive, the

¹We use the terms battery and storage unit interchangeably in this paper

storage units must collectively absorb $|r(t)|$ units of energy; when the signal is negative, they must collectively discharge $|r(t)|$ units of energy to provide the required regulation. The repeated charging and discharging of the storage units leads to degradation of battery health, which in turn reduces their operational lifetime. This degradation is commonly characterized in terms of cycling behavior, with battery lifetime measured by the number of chargedischarge cycles that can be sustained before the usable capacity degrades beyond acceptable limits.

The goal is to intelligently schedule these multiple storage units, i.e., to carry out their charge-discharge mechanism, so that the the regulation $r(t)$ is distributed across these N storage units and it results in the least possible degradation.

2.4 Cycling Degradation Model

Battery degradation due to chargedischarge cycling is highly dependent on the depth and frequency of SoC cycle that gets formed. A widely used and experimentally validated approach to quantifying cycling degradation is the rainflow cycle counting algorithm, which decomposes an SoC trajectory into chargedischarge cycles and assigns damage based on each cycles depth of discharge (DoD)².

Let $\Phi(b_i(\cdot))$ denote the set of cycles identified from the SoC trajectory $b_i(\cdot)$ of battery i , and let δ denote the DoD of a given cycle. The degradation incurred by that cycle is modeled using a stress function $f(\delta)$, which is typically nonlinear and increasing in δ . We adopt the battery degradation model in [12, 15] where the stress function $f(\delta)$ takes a polynomial form as $f(\delta) = \alpha e^{\beta\delta} \in (0, 1)$, where α and β are constants which are specific to the battery chemistry and can be inferred from the battery data sheets provided by the battery manufacturer. The total cycling degradation of battery i over a horizon T is given by

$$D_i(T) = \sum_{\delta \in \Phi(b_i(\cdot))} f(\delta). \quad (7)$$

The fleet-wide degradation is then $D(T) = \sum_{i=1}^T D_i(T)$. While tractable, this degradation model is inherently non-Markovian, as cycle identification depends on the entire SoC trajectory rather than on instantaneous state transitions. This presents a fundamental challenge for control and learning: cycles may overlap and complete at different time instants, making degradation a delayed and path-dependent quantity.

2.5 Control Objective

The system objective is to operate the batteries over a time horizon T so as to minimize the total cycling degradation

²Although battery degradation is influenced by several factors, including temperature, C-rate, average state of charge, battery chemistry, and electrochemical aging mechanisms, prior studies have shown that cycling behavior is a primary driver of degradation in applications involving frequent chargedischarge operation [22]. Therefore, we restrict attention to cycle-induced degradation in this work, while acknowledging that accounting for the comprehensive degradation modeling lies beyond the scope of this paper.

while providing frequency regulation:

$$\min_{\{a(t)\}_{t=0}^{T-1}} \sum_{i=1}^N L_i \quad (8)$$

subject to SOC dynamics (2), individual battery constraints (3) and (6), collective regulation constraint (6). The decision variables are the sequence of action vectors $a(0), a(1), \dots, a(T-1)$, wherein action vector $a(t) = (a_1(t), \dots, a_N(t))$ satisfies action constraints (1) and (6) during every time step.

2.6 Why a Sequential Decision-Making Framework Is Needed

Although the objective in (8) is well defined, it is not amenable to greedy optimization. The degradation incurred by a battery depends on entire SoC trajectories, not on instantaneous actions. An action that appears benign in the short term may contribute to deep cycles later, while a slightly more aggressive action now may prevent large cycles in the future.

This delayed and history-dependent structure makes the problem inherently sequential and motivates a Markov Decision Process (MDP) formulation, which is developed in the next section.³

Since the degradation is cycle based, it is not immediately clear how the current choice of action $a(t)$ affects the SoC cycle formation across the N batteries in the future. Consequently, any greedy policy, which choose the action with least associated degradation, will only consider whether or not an immediate cycle(s) is getting formed in the current time slot by the chosen action when it applied. Such policies are myopic and completely ignores the foresightedness of current good (greedy) action being detrimental in the future if it leads to large cycling degradation.

This motivates us go for Markov decision processes (MDP) approach where such temporal dependence of action on the reward obtained is well addressed (see [17]). The MDP model is discussed in the next subsection.

3 DEGRADATION-AWARE LEARNING FRAMEWORK

In this section, we cast the coordinated battery scheduling problem as a Markov Decision Process (MDP) and design a reward function that incentivizes long-term degradation-aware behavior. The MDP formulation enables the learning agent to account for the temporal coupling between present actions and future battery cycling behavior.

3.1 MDP model

We consider an infinite-horizon, discounted MDP defined by the tuple $(\mathcal{S}, \mathcal{A}, \mathcal{P}, \mathcal{R}, \gamma)$, where \mathcal{S} is the state space, \mathcal{A} is the action space, \mathcal{P} denotes the state transition kernel, \mathcal{R} is the reward function, and $\gamma \in (0, 1)$ is the discount factor.

³Note that even though the cycle formation is history dependent and hence non-Markovian, we analysed the problem through the MDP framework by appropriately designing a surrogate reward function that can capture the non-Markovian, history-dependent nature of cycle formation (see details in Section 3).

State Space. The system state at time t is defined as

$$s(t) = (b_1(t), b_2(t), \dots, b_N(t), r(t)) \in \mathcal{S},$$

which captures the SoC of all batteries and the current regulation request. Each battery state $b_i(t)$ takes integer values in $\{0, 1, \dots, B_i\}$ and the regulation signal $r(t)$ takes values in the finite set \mathcal{S}_r . Since energy is measured with fine granularity, discretization introduces no loss of modeling fidelity while ensuring a finite state space. The full state space is given by $\mathcal{S} = \prod_{i=1}^N \{0, 1, \dots, B_i\} \times \mathcal{S}_r$, with cardinality $|\mathcal{S}| = \left(\prod_{i=1}^N (B_i + 1)\right) |\mathcal{S}_r|$.

Action Space. An action at time t is the vector $a(t) = (a_1(t), \dots, a_N(t))$ where $a_i(t) \in \mathbb{Z}$ represents the energy charged to or discharged from battery i during time slot t . The set of feasible actions $A_{s(t)} \in \mathbb{Z}^N$ is state dependent and consists of all action vectors satisfying: individual ramp-rate and capacity constraints (1)(3), the collective regulation tracking constraint (6). The state dependence of $\mathcal{A}_{(\cdot)}$ significantly increases the complexity of the problem, as the number of feasible actions varies with the SoC configuration.

State Transitions. The state transition mechanism has two components

- (1) Battery dynamics: Given $s(t)$ and $a(t)$, the battery SoC evolves deterministically via (2)
- (2) Regulation signal dynamics: The regulation signal $r(t)$ evolves as a DTMC over state space \mathcal{S}_r with unknown transition probabilities.

Thus, the transition kernel $P(s(t+1)|s(t), a(t))$ is Markovian but unknown, making model-free RL appropriate.

Reward function. The MDP reward $R(s, a, s')$ is the reward that the environment offers to the agent when the environment transitions from s to s' under the influence of action a taken. The reward structure has the following characteristics: The immediate reward is designed to reflect the long-term objective of minimizing cycling degradation. However, since true degradation cannot be computed incrementally, the reward function is constructed using a proxy based on real-time properties of SoC trajectories. The detailed reward design is presented in Section 3.4.

3.2 Objective and Value Function

In the MDP setting, the objective of the aggregator is to find a policy π that selects actions $a(t) = \pi(s(t))$ at each time t so as to minimize the expected long-term degradation, by maximizing the MDP discounted return:

$$\max_{\pi} \mathbb{E} \left[\sum_{t=0}^{\infty} \gamma^t R(s(t), a(t), s(t+1)) \right].$$

The corresponding stateaction value function (Q-function) under policy π is defined as

$$Q^{\pi}(s, a) = \mathbb{E}_{\pi} \left[\sum_{t=0}^{\infty} \gamma^t R(s(t), a(t), s(t+1)) \mid s(0) = s, a(0) = a \right],$$

which expresses long-term performance as the immediate reward plus the discounted optimal value of the next state.

As discussed in Section 2, the true objective of the aggregator is to minimize long-term cycling degradation, which depends on chargedischarge cycles identified from the SoC trajectories of individual batteries. However, as mentioned, cycle-based degradation models such as rainflow counting are inherently non-Markovian and do not admit a natural per-time-step cost representation. This poses a challenge in designing an appropriate MDP reward function that assigns a reward (or penalty) at each time step.

3.3 Challenges in MDP Reward Design

Because cycle-based degradation is defined only upon cycle completion, an ideal reward function $R(s, a, s')$ would assign a degradation penalty to action a only for those transitions (s, a, s') where a cycle-counting procedure (such as rainflow counting algorithm) identifies a completed cycle and computes its depth of discharge; otherwise $R(s, a, s') = 0$. Formally, if a degradation cost $f(\delta)$ is incurred only when a cycle of depth δ is identified, then the instantaneous reward is zero for most time steps and nonzero only at cycle-completion events.

Such a reward structure yields a sparse and delayed learning signal, since penalties arrive only after extended sequences of actions that collectively form a cycle. Learning under this type of feedback is computationally inefficient and unstable in reinforcement learning, particularly in large state spaces. These observations motivate the design of a dense proxy reward that provides informative feedback at every time step while remaining aligned with the long-term objective of reducing cycling degradation.

3.4 Degradation-Aware MDP Reward Design

To design a dense reward that reflects long-term cycling degradation, we exploit structural properties of charge–discharge cycles formed by state-of-charge (SoC) trajectories. Cycle-based degradation models, such as rainflow counting, identify cycles between successive local maxima and minima of the SoC profile. However, cycles of different depths may overlap in time: a large-amplitude cycle can complete and be removed while a smaller-amplitude cycle, initiated earlier, remains unclosed. Figure 1 illustrates such overlapping and nested cycle formations.

This observation motivates tracking the progression of ongoing cycles using information that can be computed online, without access to future SoC values. In particular, we use switching points⁴, which correspond to local extrema of the SoC trajectory and serve as reference points for measuring the depth of incomplete cycles.

For each battery i , let $b_i^{\text{SP}}(t)$ denote the most recent switching point of its SoC trajectory prior to time t . If the SoC is currently increasing, $b_i^{\text{SP}}(t)$ corresponds to the most recent local minimum; if the SoC is decreasing, it corresponds to

⁴A switching point (or turning point) is the SOC value that defines either a local peak or a local valley in the SOC profile.

the most recent local maximum. Switching points can be detected and updated incrementally by monitoring changes in the direction of SoC evolution, making them suitable for real-time learning and control.

For each battery i , the switching point $b_i^{SP}(t)$ is defined as the most recent local extremum of its SoC trajectory prior to time t . Specifically, if the SoC trajectory is currently increasing, the switching point corresponds to the most recent local minimum; if the SoC trajectory is currently decreasing, the switching point corresponds to the most recent local maximum. Switching points can be updated incrementally by monitoring changes in the direction of SoC movement, without requiring access to future information. This makes them well suited for real-time learning and control.

The quantity $|b_i(t) - b_i^{SP}(t)|$ represents the current magnitude of SoC deviation from the most recent switching point for battery i . This deviation serves as a key indicator of the depth of the chargedischarge cycle that is currently being formed.

We now construct a dense reward function that penalizes large deviations of the SoC from switching points and thereby encourages shallow cycling behavior. For each battery i , we define the instantaneous degradation proxy reward as

$$r_i(t) = - \left(\sum_{i=1}^N \alpha_d e^{\beta|b_i(t) + a_i(t) - b_i^{SP}(t)|} - \alpha_d e^{\beta|b_i(t) - b_i^{SP}(t)|} \right), \quad (9)$$

where α, β are the degradation parameters. The MDP one step reward at time t is given by

$$R(s(t), a(t), s(t+1)) = \sum_i^N r_i(t). \quad (10)$$

The negative sign reflects the interpretation of the reward as a degradation penalty: maximizing cumulative reward corresponds to minimizing cumulative degradation. This reward-shaping mechanism incentivizes the learning agent to distribute regulation effort across batteries in a manner that avoids deep SoC deviations in any single unit, thereby reducing the formation of high-depth cycles over time.

Note that the proxy reward does not compute true cycling degradation. Instead, it serves as a surrogate objective whose minimization empirically leads to SoC trajectories with lower rainflow-counted degradation. In other words, the objective of the MDP is defined in terms of a proxy reward that is correlated with, but not identical to, cycle-based degradation. True cycle-based degradation is computed only during evaluation of the trained RL agent, as described and reported in simulation Section 5.

Connection of MDP Reward to Cycle-Based Degradation

A switching point (or turning point) in an SoC trajectory corresponds to a local maximum or minimum and marks a change in the direction of SoC evolution. In cycle-counting methods such as rainflow counting, completed chargedischarge

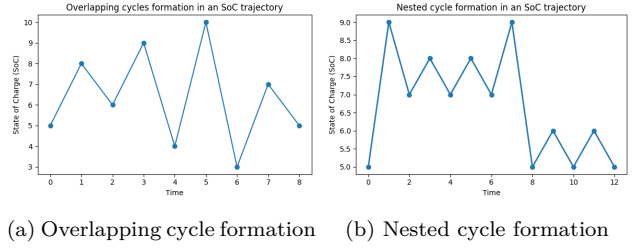


Figure 1: Illustration of overlapping and nested cycle formation in battery state-of-charge trajectories.

cycles are identified between successive switching points, and the depth of discharge (DoD) of a cycle is determined by the difference between the associated extrema. Intuitively, the quantity $|b_i(t) - b_i^{SP}(t)|$ tracks the partial depth of a developing cycle. Penalizing growth in this quantity intuitively encourages the controller to reverse direction earlier, distribute regulation across batteries, avoid concentrating large excursions on a subset of units. As a result, the learned policy implicitly shapes the SoC trajectories to reduce the frequency and depth of cycles detected by rainflow counting.

3.5 Real-Time Tracking of Switching Point $b_i^{SP}(t)$ and Cycle Evolution

The reward design in Section 3.4 relies on the most recent switching point $b_i^{SP}(t)$ of each battery's state-of-charge (SoC) trajectory. While switching points are defined as local extrema of the SoC profile, their evolution over time is more subtle than a simple forward update. In particular, when cycles overlap or get nested, the effective switching point relevant for degradation assessment may move backward along the SoC trace.

To understand this behavior, recall that charge-discharge cycles are formed between successive extrema of the SoC trajectory. In practical operation, cycles of different amplitudes may coexist: a smaller cycle can be initiated and completed within a larger excursion that has not yet closed. When such an inner cycle completes, the extrema that define it are removed from consideration, while the larger, enclosing cycle continues to evolve.

As a consequence, when a completed cycle is removed, the most recent relevant switching point for the remaining incomplete cycle may correspond to an earlier extremum along the SoC trajectory. In this sense, the switching point $b_i^{SP}(t)$ associated with the ongoing cycle can move backward in time as cycles are completed and discarded. This backward movement is a natural outcome of cycle extraction and is essential for correctly tracking the partial depth of the remaining cycle.

For real-time operation, it is therefore necessary to maintain a persistent list of switching points detected along the SoC trajectory up to the current time. At each time step, newly observed SoC values may generate new extrema, which

are appended to this list. When a cycle completes, the extrema defining that cycle are removed, potentially exposing an earlier switching point as the active reference for the ongoing cycle. The current switching point $b_i^{SP}(t)$ is then defined as the most recent extremum associated with the incomplete cycle that remains after this removal process.

Importantly, although this procedure is inspired by cycle-counting principles, it operates incrementally and does not require access to future SoC values. At every time step, the maintained switching-point structure provides the correct reference $b_i^{SP}(t)$ needed to compute the one-step MDP reward in (9)-(10). In this way, the reward reflects the instantaneous growth of the active cycle, even as the underlying cycle structure evolves dynamically over time.

During the performance evaluation of the trained agent, we use complete offline SoC trajectories and standard cycle-counting methods. During learning and control, the switching-point tracking mechanism serves solely to support the construction of a dense, real-time reward that remains aligned with cycle-based degradation.

4 DEGRADATION-AWARE SCHEDULING VIA REINFORCEMENT LEARNING

In this section, we present the reinforcement learning (RL) methods used to obtain degradation-aware scheduling policies. We first describe a tabular Q -learning approach, which is suitable for small problem instances, and then introduce a scalable function-approximation-based method using Extreme Learning Machines (ELMs) for large stateaction spaces.

4.1 Tabular Q -Learning for Small-Scale Systems

For finite MDPs, Q -learning is a classical reinforcement learning algorithm. Let π denote a stationary policy that maps states to feasible actions. The action-value function associated with policy π is defined as

$$Q^\pi(s, a) = \mathbb{E} \left[\sum_{t=0}^{\infty} \gamma^k R(s(t), \pi(s(t)), s(t+1)) \middle| s(0) = s, a(0) = a \right].$$

The optimal action-value function $Q^*(s, a)$ satisfies the Bellman optimality equation (see [17]), given by

$$Q^*(s, a) = \mathbb{E} \left[R(s, a, s') + \gamma \sum_{s' \in \mathcal{S}} P(s'|s, a) \max_{a' \in \mathcal{A}_{s'}} Q^*(s', a') \right].$$

where s' is the successor state resulting from applying action a in state s and $P(s'|s, a)$ is the probability of this state transition under the influence of action a . This recursive relationship facilitates learning of optimal policies in finite MDPs.

Since the transition probabilities of the regulation signal are unknown, we employ model-free Q -learning, which iteratively updates Q -values using observed transitions:

$$Q(s(t), a(t)) \leftarrow Q(s(t), a(t)) + \alpha(t) \left\{ R(s(t), a(t), s(t+1)) + \gamma \max_a Q(s(t+1), a) - Q(s(t), a(t)) \right\} \quad (11)$$

where $\alpha(t) \in (0, 1)$ is the learning rate.

The conversion of $Q(s, a)$ to optimal Q -values $Q^*(s, a)$, using the above update⁵, is guaranteed if the learning rate $\alpha(\cdot)$ satisfies following classical RobbinsMonro conditions for stochastic approximation (see [17])

$$\sum_t \alpha(t) = \infty, \quad \sum_t \alpha^2(t) < \infty. \quad (12)$$

The converged Q functions or the Q -values obtained using (11) are then used to infer the RL policy as

$$\pi_{Q \text{ learning}}(s) = \arg \max_{a \in \mathcal{A}} Q(s, a).$$

4.2 Limitations of Tabular Q -Learning

Although conceptually simple, tabular Q -learning becomes impractical in our setting when, battery capacities are large,energy is discretized finely, or the number of batteries increases. In fact, the number of stateaction pairs grows exponentially with N^6 , making storage and convergence of the Q -table computationally infeasible. This motivates the use of function approximation wherein the aim is to approximate the Q -function via some function approximation technique.

4.3 Function Approximation for Large StateAction Spaces

To address the curse of dimensionality, we approximate the action-value function using a linear function approximator:

$$\hat{Q}(s, a; w) = w^\top \phi(s, a), \quad (13)$$

where $\phi(s, a) \in \mathbb{R}^d$ is a feature vector extracted from the state-action pair, and $w \in \mathbb{R}^d$ is a parameter vector to be learned.

The parameters are updated using a stochastic semi-gradient method:

$$w \leftarrow w + \alpha_t \left(R(s, a, s') + \gamma \max_{a' \in \mathcal{A}(s')} \hat{Q}(s', a'; w) - \hat{Q}(s, a; w) \right) \phi(s, a). \quad (14)$$

The quality of approximation and hence the learning performance depend critically on the choice of feature map $\phi(\cdot, \cdot)$, which we describe next.

⁵with an exploratory policy that ensures every state-action pair is sufficiently explored

⁶recall from MDP model in Section 3.1 that the cardinality of state space alone grows as $|\mathcal{S}| = (\prod_{i=1}^N (B_i + 1)) |\mathcal{S}_r|$.

4.4 Feature Extraction via Extreme Learning Machines

Designing effective nonlinear features for reinforcement learning is challenging, particularly in systems with strong coupling between actions and state evolution, such as battery scheduling. To capture these nonlinearities, deep neural networks can be used, but they introduce training instability and significant computational overhead. To balance expressiveness and stability, we employ Extreme Learning Machines (ELMs) as nonlinear feature extractors [6].

4.4.1 ELM Architecture. An ELM is a single-hidden-layer feed-forward neural network in which the input-layer weights and biases are randomly initialized and fixed, and only the output-layer weights are learned.

Let $x \in \mathbb{R}^p$ denote the input vector to the ELM. In our setting, we use

$$x = [s, a, r, b_i^{SP}(t)], \quad (15)$$

i.e., the concatenation of the state vector, action vector, current reward obtained, and the vector of most recent switching points across N battery units, resulting in $p = 3N + 2$.

The hidden-layer output is given by

$$\phi(s, a) = \sigma(Wx + \tilde{b}), \quad (16)$$

where $W \in \mathbb{R}^{d \times p}$ is a randomly initialized weight matrix, $\tilde{b} \in \mathbb{R}^d$ is a bias vector, $\sigma(\cdot)$ is an elementwise activation function (e.g., sigmoid or ReLU), and d is the number of hidden units.

The hidden layer output of the ELM, $\phi(s, a)$, serves as the feature vector in the linear Q-function approximation in (13).

4.4.2 Why ELMs Are Suitable in This Setting. The use of ELM-based features is well suited to the present setting for several reasons. Random projections combined with nonlinear activation map stateaction pairs into a high-dimensional feature space in which linear value-function approximation is effective. Because the input-layer weights are fixed, learning reduces to a linear stochastic approximation problem, avoiding the instability often associated with backpropagation-based reinforcement learning. In addition, feature computation is inexpensive and parameter updates scale linearly with the number of features, making the approach computationally efficient.

Additionally, Theorem 2.2 in [6] establishes that for a single-hidden-layer network with an infinitely differentiable activation function and randomly initialized input-layer weights and biases, the induced ELM feature map is universal in the following sense: for any finite dataset $\{(s_i, a_i)\}_{i=1}^M$ with targets $Q_{\text{target}}(s_i, a_i)$ and any $\epsilon > 0$, there exists a set of output weights w such that $\frac{1}{M} \sum_{i=1}^M (Q_{\text{target}}(s_i, a_i) - w^\top \phi_{\text{ELM}}(s_i, a_i))^2 < \epsilon$. Although derived in a supervised learning context, this result provides theoretical justification for using randomized nonlinear feature maps together with linear value-function approximation in the present reinforcement learning setting.

4.4.3 Initialization and Parameters. The weights W and biases \tilde{b} are initialized independently and identically distributed from a uniform distribution over $[-1, 1]$. The output weights w are initialized to zero. The feature dimension d is chosen to balance approximation accuracy and computational complexity.

After training (elaborated in Section 4.5), the function-approximation-based policy is given by

$$\pi_{\text{FA}}(s) = \arg \max_{a \in \mathcal{A}(s)} \hat{Q}(s, a; w). \quad (17)$$

This policy selects, at each state, the feasible action satisfying (1), (3), (6) that maximizes the estimated long-term degradation-aware value.

4.5 RL Training Algorithm

We now describe the training procedure used to learn the function-approximation-based degradation-aware scheduling policy. The learning algorithm builds on the semi-gradient temporal-difference update in (14), combined with experience replay and minibatch updates to improve stability and sample efficiency.

Experience Collection and Replay Buffer. During training, the agent interacts with the environment by observing state transitions of the form $(s(t), a(t), R(t), s(t+1))$. Each such transition is stored in a replay buffer. The replay buffer is used to randomly sample past experiences when updating the value-function parameters, thereby reducing temporal correlations between successive updates and improving the stability of learning.

Mini-batch Semi-Gradient Updates. Rather than updating the parameter vector w using a single transition, we employ mini-batch updates. At each update step, a batch of N_{batch} transitions is sampled uniformly at random from the replay buffer. The parameter vector is then updated by averaging the temporal-difference (TD) errors across the batch:

$$w \leftarrow w + \frac{\alpha_t}{N_{\text{batch}}} \sum_{i=1}^{N_{\text{batch}}} \left(R(s_i, a_i, s'_i) + \gamma \max_{a' \in \mathcal{A}(s'_i)} \hat{Q}(s'_i, a'; w) - \hat{Q}(s_i, a_i; w) \right) \phi(s_i, a_i). \quad (18)$$

Batch updates reduce the variance of parameter updates and mitigate the effect of noisy individual transitions.

Exploration Strategy. To ensure sufficient exploration of the state action space, actions are selected using an ϵ -greedy policy during training. With probability ϵ_t , the agent selects a feasible action uniformly at random from $\mathcal{A}_{s(t)}$, and with probability $1 - \epsilon_t$, it selects the action that maximizes the estimated action-value function. The exploration parameter ϵ_t decays over time according to a predefined schedule to gradually shift from exploration to exploitation.

Learning Rate and Practical Considerations. The learning rate α_t is chosen to decrease over time to promote stable learning. While classical RobbinsMonro conditions in (12)

Table 1: Performance comparison under the toy Markov regulation model ($\mathcal{S}_r = \{-4, -1, 1, 5\}$, $T = 10^5$, $c_1 = d_1 = 2$, $c_2 = d_2 = 3$). Accumulated rewards and per-battery cycling degradation (D_1, D_2) are reported for each policy.

(B_1, B_2)	$ \mathcal{S} \times \mathcal{A} $	Policy Performance					
		Naive Policy		Greedy Policy		RL-ELM Policy	
		Reward	Degradation (D_1, D_2)	Reward	Degradation (D_1, D_2)	Reward	Degradation (D_1, D_2)
(2,3)	420	-14.17	(0.17, 0.17)	-3.89	(0.05, 0.05)	-1.66	(0.02, 0.0198)
(3,5)	840	-41.64	(0.16, 0.15)	-28.41	(0.18, 0.10)	-24.57	(0.19, 0.1567)
(10,10)	4235	-50.46	(0.17, 0.13)	-47.27	(0.24, 0.23)	-44.88	(0.10, 0.0575)
(15,10)	6160	-47.27	(0.15, 0.13)	-44.34	(0.11, 0.29)	-38.32	(0.09, 0.0536)
(20,20)	15435	-29.77	(0.15, 0.11)	-27.28	(0.19, 0.19)	-26.01	(0.07, 0.0406)
(25,25)	23660	-23.97	(0.15, 0.11)	-21.95	(0.17, 0.18)	-20.74	(0.07, 0.0398)
(30,30)	33635	-20.31	(0.15, 0.11)	-18.81	(0.18, 0.17)	-17.09	(0.07, 0.0242)
(40,40)	58835	-15.16	(0.16, 0.11)	-13.94	(0.17, 0.17)	-12.58	(0.06, 0.0296)
(50,50)	91035	-12.23	(0.15, 0.11)	-11.34	(0.19, 0.17)	-9.90	(0.07, 0.0348)

provide theoretical guidance for stochastic approximation, we note that the use of function approximation and experience replay prohibits strict convergence guarantees [14, 17]. Nevertheless, empirically decaying step sizes are observed to yield stable learning behavior in our setting (see Section 5).

Input Normalization and Activation Function. The inputs to the ELM feature extractor comprising regulation signal, battery SoC levels and actions are normalized to comparable scales to improve numerical conditioning and learning stability. We find that such normalization of input is quite common in neural network-based learning, which significantly improves performance [1]. Among various activation functions tested, the Sigmoid Linear Unit (SiLU) consistently yields better empirical performance than ReLU in our experiments, likely due to its smoother nonlinearity. Wider literature also finds the Sigmoid Linear Unit to show better performance while approximating continuous functions [4, 16].

Training and Policy Extraction. Training is performed over multiple episodes, each corresponding to a long realization of the regulation signal. After training converges, the learned parameter vector w is fixed, and the degradation-aware policy is obtained by greedily selecting, at each state, the feasible action that maximizes the approximated action-value function:

$$\pi_{\text{FA}}(s) = \arg \max_{a \in \mathcal{A}(s)} \hat{Q}(s, a; w).$$

The specific hyperparameter values and training configurations used in the experiments are reported in Section 5.

5 EXPERIMENTAL EVALUATION

In this section, we evaluate the proposed degradation-aware reinforcement learning (RL) framework using both synthetic and real-world regulation signals. The evaluation focuses on two questions: Does the learned policy reduce cycle-based battery degradation compared to reward-agnostic baselines, and can the proposed function-approximation-based RL method scale to realistic problem sizes? We answer these questions

by comparing accumulated rewards and post hoc cycle statistics obtained via rainflow counting.

5.1 Experimental Setup

5.1.1 Time Horizon and Granularity. All experiments are conducted over long horizons to ensure sufficient cycle formation. Unless stated otherwise, the time horizon is $T = 10^5$ time steps. Energy is measured with fine granularity so that all state and action variables are integer-valued.

5.1.2 Battery Configuration. We consider systems with $N = 2$ heterogeneous batteries. Each experiment specifies: battery capacities (B_1, B_2), charge and discharge limits (c_i, d_i), and a fixed control interval duration T steps. While the experiments focus on two batteries for clarity, the learning framework directly generalizes to larger N .

5.1.3 Agents Compared. To assess the benefits of degradation-aware learning/training, we compare the proposed reinforcement learning agents against two baseline agents that do not explicitly consider cycling degradation.

Reward-Agnostic Naive Agent. A simple baseline that allocates the regulation signal in proportion to battery capacities:

$$a_i(t) = \left\lfloor \frac{B_i}{\sum_{j=1}^N B_j} r(t) \right\rfloor, \quad (19)$$

with any rounding mismatch allocated to a feasible battery so as to satisfy (1) and (6). Specifically, the remaining energy resulting from the floor operation is allocated, one unit at a time, to feasible batteries selected uniformly at random. At each allocation step, the feasible set consists of batteries that satisfy the ramp and state-of-charge constraints (1), (6) and have sufficient headroom (for charging) or available energy (for discharging).

Greedy Agent. Another myopic policy that chooses the action based on one one-step MDP reward as

$$a(t) = \max_{a(t) \in \mathcal{A}_{s(t)}} R(s(t), a(t), s(t+1)) \quad (20)$$

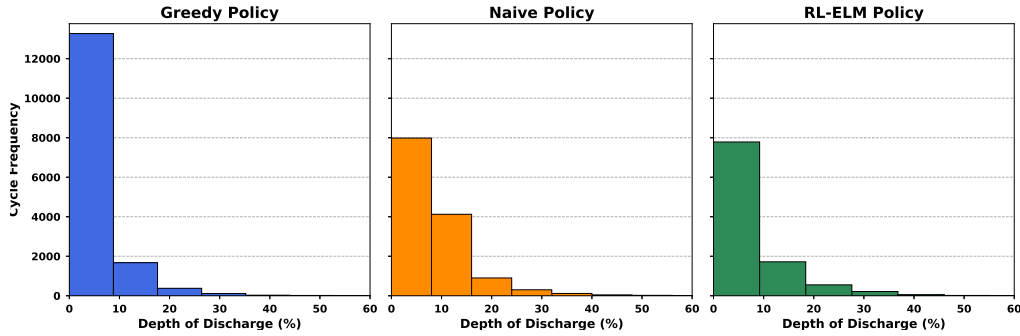


Figure 2: Distribution of cycle occurrence across DoD levels under different control policies in battery of size $B = 25$.

These two baselines serve as reference points for evaluating the benefits of learning degradation-aware policies. We compare these baselines with two RL agents—tabular Q-learning (only for small state spaces) and a function approximation-based RL agent (ELM-RL) that uses ELM-based feature extraction and linear Q -function approximation.

RL training details. The RL agents use an ϵ -greedy exploration strategy during training, with a decaying exploration rate as $\epsilon_t = \frac{\epsilon}{1+0.005t}$, with $\epsilon = 0.6$. As mentioned in Section 4.5, the learning rate α_t is varied as $\alpha_t = \frac{\alpha}{N_t(s,a)}$, where $\alpha = 10^{-4}$ and $N_t(s,a)$ is the number of times the currently encountered state-action pair (s,a) has been visited till time step t . A minibatch of size $N_{batch} = 128$ is used to update the weights w every 8 samples or interaction with the environment during RL training. This minibatch is sampled from the reply buffer whose size is kept as 2000 for the toy setting and 160,000 for the simulation with PJM trace.

5.1.4 Performance Metrics. We report the accumulated reward $R^\pi = \sum_{t=0}^{T-1} R(s(t), a(t), s(t+1))$, along the sample path of the evolved state trajectory $\{s(t)\}_{t=0}^{T-1}$ over which we want to evaluate the performance of the RL agent and other baseline agents. We also report cycle statistics obtained from rainflow counting, including: number of cycles, depth-of-discharge (DoD) histograms, total degradation computed using the stress function in (7).⁷ These latter metrics are computed offline using the full state-of-charge trajectories and represent the true performance objective.

5.2 Synthetic Regulation Signal (Toy Markov Model)

We first evaluate the agents using a small synthetic discrete-time Markov chain (DTMC) to validate learning behavior under controlled conditions.

5.2.1 Signal Model. The regulation signal evolves over the finite state space $S_r = \{-4, -1, 1, 5\}$, with a fixed transition probability matrix. The transition matrix is used only to generate the signal trajectory and is unknown to all agents.

⁷We use the stress function $(k_{\delta_1}\delta^{k_{\delta_2}} + k_{\delta_3})^{-1}$ with $k_{\delta_1} = 1.4 \times 10^5$, $k_{\delta_2} = -5.01 \times 10^{-1}$, and $k_{\delta_3} = -1.23 \times 10^5$. These constants can be found in [22].

5.2.2 Battery Parameters. We consider two batteries with identical ramp limits,

$$c_1 = d_1 = 2, c_2 = d_2 = 3, \quad (21)$$

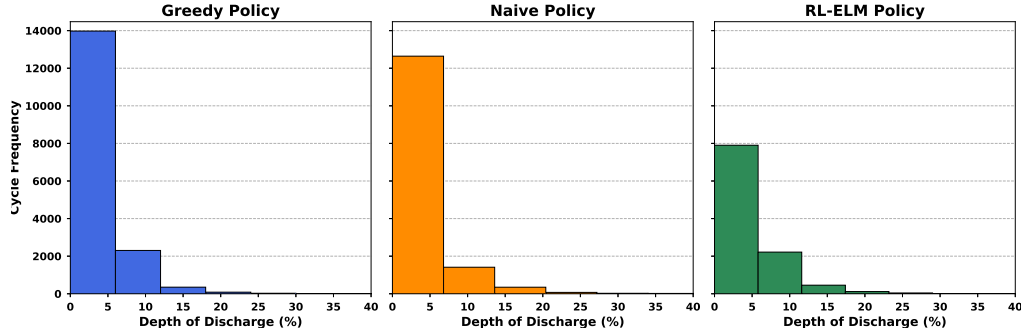
and vary the capacities (B_1, B_2) across experiments.

5.2.3 Results. For various battery size configurations (B_1, B_2) , each defining an MDP instance, the accumulated reward obtained with RL agents and with other baseline naive agents is reported in Table 1. Across all battery size configurations (see Table 1), the reinforcement learning agents outperform the naive baseline in terms of accumulated reward. The function-approximation-based RL agent consistently achieves the highest reward, indicating lower degradation. To interpret these results physically, we examine rainflow-counted cycle statistics. As reported in Table 1, the actual cycling degradation computed offline (after the simulation using the full SoC trajectory) using the rainflow counting algorithm is less in both battery units compared to the operation carried out by the baseline naive and greedy policies. The learned RL policy reduce the number of deep cycles, redistribute regulation effort across batteries, and induce more shallow cycling behavior. Histograms of cycle depth (see Fig. 2 and 3) show a clear reduction in both the frequency and magnitude of high depth-of-discharge (DoD) cycles under RL control. These trends directly explain the higher accumulated reward and lower total degradation.

5.3 Evaluation with PJM RegD Frequency Regulation Signal

To validate performance under a realistic regulation signal, we evaluate the proposed framework using historical PJM RegD data. The data was collected during the University of Delaware vehicle-to-grid (V2G) field demonstration in Spring 2013 (see here [8]). The dataset consists of a high-resolution RegD signal sampled at 10-second intervals and reflects the fast, zero-mean regulation service request deployed by PJM.

5.3.1 Experimental Details. The RegD signal is normalized with respect to a regulation capacity of $A_{Reg} = 10$ kWh, such that a normalized value of +1 corresponds to a request for +10 kWh of charging over a control interval, while a value of -1 corresponds to -10 kWh of discharging. We sample

Figure 3: Distribution of cycle occurrence across DoD levels under different control policies in battery of size $B = 50$.Table 2: Performance comparison under the PJM Regulation Data ($c_1 = d_1 = 5$, $c_2 = d_2 = 10$, ELM feature dimension $d = 50$). Accumulated rewards and per-battery cycling degradation (D_1, D_2) are reported for each policy.

(B_1, B_2)	$ \mathcal{S} \times \mathcal{A} $	Policy Performance					
		Naive Policy		Greedy Policy		RL-ELM Policy	
		Reward	Degradation (D_1, D_2)	Reward	Degradation (D_1, D_2)	Reward	Degradation (D_1, D_2)
(5, 10)	15,246	-5.89	(0.003732, 0.006304)	-4.64	(0.003516, 0.003785)	-4.64	(0.003516, 0.003785)
(10, 10)	27,951	-7.01	(0.006284, 0.006208)	-5.81	(0.004136, 0.00526)	-5.79	(0.004295, 0.005343)
(15, 10)	40,656	-7.44	(0.007506, 0.006245)	-6.46	(0.004689, 0.005918)	-6.46	(0.004689, 0.005918)
(15, 20)	77,616	-7.96	(0.007325, 0.008113)	-7.18	(0.007067, 0.005162)	-7.18	(0.007067, 0.005162)
(20, 20)	101,871	-8.12	(0.008053, 0.008087)	-7.37	(0.00603, 0.006304)	-7.37	(0.005754, 0.006407)
(20, 30)	150,381	-8.20	(0.008029, 0.008635)	-7.60	(0.00742, 0.005628)	-7.60	(0.00742, 0.005628)
(30, 30)	221,991	-8.26	(0.008608, 0.008592)	-7.73	(0.0064, 0.006215)	-7.73	(0.006086, 0.006176)
(50, 50)	600,831	-8.04	(0.008742, 0.008436)	-7.69	(0.005412, 0.005349)	-7.67	(0.004521, 0.004756)
(75, 75)	1,334,256	-7.56	(0.008161, 0.008317)	-7.31	(0.004549, 0.004449)	-7.28	(0.003969, 0.00408)
(75, 100)	1,773,156	-7.28	(0.00762, 0.008007)	-7.06	(0.006712, 0.003731)	-7.04	(0.006107, 0.003499)
(100, 100)	2,356,431	-7.03	(0.007622, 0.007455)	-6.84	(0.004554, 0.004119)	-6.82	(0.003444, 0.003306)

the RegD signal at a resolution of 0.1, which translates to 21 possible regulation values over the trace. This stochastically varying RegD signal, spanning 109,846 samples, serves as the training and evaluation signal for the RL agent. This trajectory is treated as a single episode, allowing the learning agent to experience realistic long-term cycling behavior without artificial episode resets.

5.3.2 Results. Tables 2 report performance under the PJM RegD signal for different battery configurations across different policies. Across all MDP instances, the RL-ELM agent consistently outperforms the naive and greedy baselines in terms of accumulated reward and rainflow-counted cycling degradation. The learned policies exhibit a marked reduction in deep cycles and a more balanced distribution of regulation effort across the battery units. Note that even with as few as 10 hidden units, the RL-ELM agent maintains a substantial advantage over baseline policies.

6 CONCLUSION, LIMITATIONS, AND FUTURE WORK

This paper studied the problem of degradation-aware frequency regulation using a fleet of heterogeneous battery storage units. By formulating the control problem as a Markov

decision process with a carefully designed proxy reward, we demonstrated that reinforcement learning can systematically shape state-of-charge trajectories to reduce long-term cycling degradation under stochastic regulation signals. Extensive numerical experiments using both synthetic and real-world regulation data confirm that the proposed approach consistently suppresses deep cycles and lowers degradation compared to baseline dispatch policies.

Several limitations of the present work point to promising directions for future research. While frequency regulation tracking requirements are enforced through hard feasibility constraints on the action space, explicit penalties for regulation error are not directly incorporated into the MDP reward. A natural extension is to integrate tracking performance and degradation costs within a unified reward structure, enabling a more explicit exploration of the trade-off between regulation accuracy and battery lifetime.

The present model focuses exclusively on cycle-induced degradation and does not explicitly account for other aging mechanisms such as calendar aging, temperature effects, or rate-dependent losses. Incorporating degradation models that capture these additional factors, while maintaining tractability for online learning, remains an important open challenge.

REFERENCES

[1] Christopher M. Bishop. 2006. *Pattern Recognition and Machine Learning*. Springer, New York.

[2] Jun Cao, Dan Harrold, Zhong Fan, Thomas Morstyn, David Healey, and Kang Li. 2020. Deep Reinforcement Learning-Based Energy Storage Arbitrage With Accurate Lithium-Ion Battery Degradation Model. *IEEE Transactions on Smart Grid* 11, 5 (2020), 4513–4521. [doi:10.1109/TSG.2020.2986333](https://doi.org/10.1109/TSG.2020.2986333)

[3] Stephen D Downing and DF Socie. 1982. Simple rainflow counting algorithms. *International journal of fatigue* 4, 1 (1982), 31–40.

[4] Duong V. Dung, Nguyen D. Song, Pramudita S. Palar, and Lavi R. Zuhal. 2023. On The Choice of Activation Functions in Physics-Informed Neural Network for Solving Incompressible Fluid Flows. In *AIAA SCITECH 2023 Forum*. [doi:10.2514/6.2023-1803](https://doi.org/10.2514/6.2023-1803)

[5] Yuhang Hao, Qiugang Lu, Xizhe Wang, and Benben Jiang. 2023. Adaptive model-based reinforcement learning for fast-charging optimization of lithium-ion batteries. *IEEE Transactions on Industrial Informatics* 20, 1 (2023), 127–137.

[6] Guang-Bin Huang, Qin-Yu Zhu, and Chee-Kheong Siew. 2006. Extreme learning machine: Theory and applications. *Neurocomputing* 70, 1 (2006), 489–501. [doi:10.1016/j.neucom.2005.12.126](https://doi.org/10.1016/j.neucom.2005.12.126) Neural Networks.

[7] Aleksandar Janjic, Lazar Velimirovic, Miomir Stankovic, and Andrija Petrusic. 2017. Commercial electric vehicle fleet scheduling for secondary frequency control. *Electric Power Systems Research* 147 (2017), 31–41.

[8] Willett Kempton and University of Delaware V2G Research Group. 2013. Fast Regulation Signal Data (PJM REG-D). University of Delaware V2G Resources. <https://www1.udel.edu/V2G/resources/Fast-Regulation-Data.csv> Accompanied by Fast-Regulation-Explanation.txt.

[9] Kyung-Bin Kwon and Hao Zhu. 2022. Reinforcement Learning-Based Optimal Battery Control Under Cycle-Based Degradation Cost. *IEEE Transactions on Smart Grid* 13, 6 (2022), 4909–4917. [doi:10.1109/TSG.2022.3180674](https://doi.org/10.1109/TSG.2022.3180674)

[10] Hui Liu, Zechun Hu, Yonghua Song, and Jin Lin. 2013. Decentralized vehicle-to-grid control for primary frequency regulation considering charging demands. *IEEE Transactions on Power Systems* 28, 3 (2013), 3480–3489.

[11] Xing Luo, Jihong Wang, Mark Dooner, and Jonathan Clarke. 2015. Overview of current development in electrical energy storage technologies and the application potential in power system operation. *Applied energy* 137 (2015), 511–536.

[12] Alan Millner. 2010. Modeling Lithium Ion battery degradation in electric vehicles. In *2010 IEEE Conference on Innovative Technologies for an Efficient and Reliable Electricity Supply*. 349–356. [doi:10.1109/CITRES.2010.5619782](https://doi.org/10.1109/CITRES.2010.5619782)

[13] Volodymyr Mnih, Koray Kavukcuoglu, David Silver, Andrei A Rusu, Joel Veness, Marc G Bellemare, Alex Graves, Martin Riedmiller, Andreas K Fidjeland, Georg Ostrovski, et al. 2015. Human-level control through deep reinforcement learning. *nature* 518, 7540 (2015), 529–533.

[14] Martin L Puterman. 2014. *Markov decision processes: discrete stochastic dynamic programming*. John Wiley & Sons.

[15] Yuanyuan Shi, Bolun Xu, Yushi Tan, and Baosen Zhang. 2018. A convex cycle-based degradation model for battery energy storage planning and operation. In *2018 Annual American Control Conference (ACC)*. IEEE, 4590–4596.

[16] Tanay Raghunandan Srinivasa and Suraj Kumar. 2025. Solving Infinite-Horizon Optimal Control Problems using the Extreme Theory of Functional Connections. In *Proceedings of the 11th Indian Control Conference (ICC)*. <https://arxiv.org/abs/2510.27187> Presented at ICC-11; also available as arXiv:2510.27187.

[17] Richard S Sutton and Andrew G Barto. 2018. *Reinforcement learning: An introduction*. MIT press.

[18] José R Vázquez-Canteli and Zoltán Nagy. 2019. Reinforcement learning for demand response: A review of algorithms and modeling techniques. *Applied energy* 235 (2019), 1072–1089.

[19] Zhiqiang Wan, Hepeng Li, Haibo He, and Danil Prokhorov. 2018. Model-free real-time EV charging scheduling based on deep reinforcement learning. *IEEE Transactions on Smart Grid* 10, 5 (2018), 5246–5257.

[20] Hao Wang and Baosen Zhang. 2018. Energy storage arbitrage in real-time markets via reinforcement learning. In *2018 IEEE Power & Energy Society General Meeting (PESGM)*. IEEE, 1–5.

[21] Florian Wankmüller, Prakash R Thimmapuram, Kevin G Gallagher, and Audun Botterud. 2017. Impact of battery degradation on energy arbitrage revenue of grid-level energy storage. *Journal of Energy Storage* 10 (2017), 56–66.

[22] Bolun Xu, Alexandre Oudalov, Andreas Ulbig, Göran Andersson, and Daniel S. Kirschen. 2018. Modeling of Lithium-Ion Battery Degradation for Cell Life Assessment. *IEEE Transactions on Smart Grid* 9, 2 (2018), 1131–1140. [doi:10.1109/TSG.2016.2578950](https://doi.org/10.1109/TSG.2016.2578950)

[23] Hongtao Zhang, Guanglin Zhang, Mingbo Zhao, and Yuping Liu. 2024. Load forecasting-based learning system for energy management with battery degradation estimation: A deep reinforcement learning approach. *IEEE Transactions on Consumer Electronics* 70, 1 (2024), 2342–2352.

[24] Yunwei Zhang, Qiaochu Tang, Yao Zhang, Jiabin Wang, Ulrich Stimming, and Alpha A Lee. 2020. Identifying degradation patterns of lithium ion batteries from impedance spectroscopy using machine learning. *Nature communications* 11, 1 (2020), 1706.